ORIGINAL RESEARCH ARTICLE

Experimental Study on the Chemical Stability of Phosphate-Bonded Al_2O_3-Based Ceramic Foam Filters (CFFs)

ARE BERGIN, CLAUDIA VOIGT, ROBERT FRITZSCH, SHAHID AKHTAR, LARS ARNBERG, CHRISTOS G. ANEZIRIS, and RAGNHILD E. AUNE

Production of high-quality aluminum products requires an extensive melt treatment process, even more so with the increasing focus on recycling and sustainability. Filtration is a commonly used process segment for removal of non-metallic inclusions in aluminum, and ceramic foam filters (CFFs) are often used as the filtration media. In the present study, the chemical stability of phosphate-bonded Al_2O_3-based CFFs has been investigated. Three filters with different chemical compositions have been submerged into pure aluminum (with traces of Mg) and in an aluminum-magnesium melt (~ 2 wt pct Mg) at 730 °C. In addition to filter characterization before and after exposure to molten metal, using various imaging and X-ray techniques, the melt itself was analyzed by spark optical emission spectroscopy. The generation of phosphine gas was also measured by the use of Dräger tubes, and thermodynamic calculations performed using FactSage™. The phosphate-bonded filters were observed to react with the magnesium present in the molten aluminum even at very low magnesium concentrations (0.00035 wt pct), and as the magnesium concentration increased the severity of the degradation became more and more evident. The exposure time proved to have detrimental effect on the filter structure, with pieces of the filter struts broken off causing melt contamination. Severe filter degradation also resulted in color changes with accompanying diffusion of magnesium and phosphorus to and from the filter, respectively. Moreover, phosphine gas was released in amounts exceeding recommended exposure limits when the filter came in contact with the humidity in the air after testing. Good agreement was established to exist between the results from the thermodynamic calculations performed and the experimental results.

https://doi.org/10.1007/s11663-021-02144-3

I. INTRODUCTION

CERAMIC foam filters (CFFs) are widely used for the removal of non-metallic inclusions from molten metal during the casting step, and they are manufactured in large quantities with the use of a replica technique that is patented by Schwartzwalder *et al.*[1] The production process of ceramic foam filters consists of several steps in which a polyurethane (PUR) foam initially is coated by a ceramic slurry, followed by removal of excess slurry and a sintering step where the polyurethane decomposes and the ceramic foam remains. The key feature of ceramic foam filters is the porosity which can be divided into three main categories: (1) functional porosity (pores surrounded by the struts), (2) material porosity (pores within the struts), and (3) strut cavities (a result from decomposition of the polymeric foam), see Figure 1.

The main introduction of ceramic foam filters into the aluminum (Al) industry occurred in the 1970s[2] followed by a number of patents specifically describing filtration of aluminum.[3–5] Today, ceramic foam filters made of calcined alumina (Al_2O_3) are typically used in this area to improve the cleanliness of the cast metal. The filter ability to remove particles and inclusions is dependent on several factors, in which perhaps the most important one is the density of the functional pores, usually denoted ppi (pores per inch). It has been reported in the

ARE BERGIN is with the Department of Materials Science and Engineering, Norwegian University of Science and Technology (NTNU), 7034 Trondheim and also with the Research and Technology Development, Hydro Aluminium AS, 6600, Sunndalsøra, Norway. Contact e-mail: are.bergin@hydro.com; are.bergin@ntnu.no CLAUDIA VOIGT and CHRISTOS G. ANEZIRIS are with the Institute of Ceramics, Refractories and Composite Materials, Technische Universität Bergakademie Freiberg, 09599 Freiberg, Germany. ROBERT FRITZSCH, LARS ARNBERG, and RAGNHILD E. AUNE are with the Department of Materials Science and Engineering, Norwegian University of Science and Technology (NTNU). SHAHID AKHTAR is with the Karmøy Primary Production, Hydro Aluminium AS, 4265, Håvik, Norway

Manuscript submitted October 6, 2020, accepted March 4, 2021.
Article published online April 22, 2021.

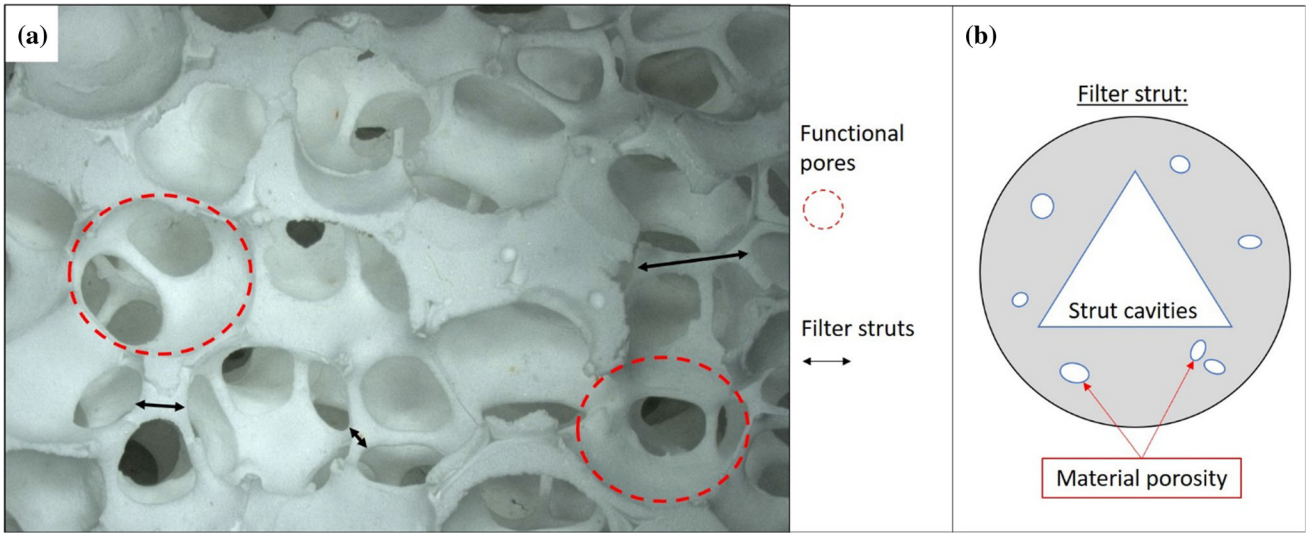

Fig. 1—A schematic presentation of pores in a ceramic foam filter: (*a*) a photograph of a filter where the functional pores and filter struts are marked, and (*b*) the strut cavity and material porosity of a filter strut.

literature that the filtration efficiency is in the range of 25 to 90 pct for 30 ppi filters and 55 to 95 pct for 50 filters.[6]

As pure Al_2O_3 has a melting point of 2050 °C,[7] the sintering temperatures of pure alumina filters are rather high, which causes an energy-intensive sintering step. Like most refractory materials, ceramic foam filters are cost sensitive which applies mostly due to their single use application. A reduction in production costs is, however, possible with the addition of an inorganic binder that reduces the sintering temperature and thereby the energy consumption. An often-used inorganic binder is phosphate, which provides excellent strength at low temperatures allowing easy product handling, and a reduction of the sintering temperature from around 1600 °C (pure alumina) to around 1300 °C. Additionally, the phosphate-bonded ceramics are suitable for fast sintering processes.[8] However, shrinkage is a negative effect of high-temperature sintering, which might deform the pores and lead to micro-crack formation especially for larger filter geometries. Due to this, suppliers tend to use slurry compositions where shrinkage is reduced to a minimum.

The constituents in the slurry of a conventional phosphate-bonded alumina ceramic foam filter are, as described in the patent by Brockmeyer,[5] 50 to 80 pct Al_2O_3, 1 to 5 pct of montmorillonite, 1 to 10 pct ceramic fibers, and 5 to 25 pct of a phosphate binder. According to Nishikawa,[8] monoaluminum phosphate ($Al(H_2PO_4)_3$) transforms to $Al(PO_3)_3$ at 315 °C with subsequent formation to a metaphosphate glass at temperatures between 1090 °C and 1300 °C, which is further transformed to $AlPO_4$ (berlinite) at temperatures between 1300 °C and 1500 °C. In the presence of alumina, the formation of $AlPO_4$ from $Al(PO_3)_3$ is accelerated and takes place at much lower temperatures, *i.e.*, between 700 °C and 1000 °C. $AlPO_4$ coats the alumina particles and thus acts as the bonding phase.[9]

In regard to phosphate-bonded ceramics, MgO has proven to act as a setting agent that accelerates the solidification of the ceramic slurry.[10] Furthermore, phosphates and magnesia can generate low-melting compounds (e.g., $Mg(PO_3)_2$ at 1165 °C), and MgO has been reported to break the aluminum phosphate bonds which decreases the mechanical strength of a ceramic foam filter at high temperatures.[10]

For the use of ceramic foam filters in other applications, such as hot gas filtration, it has been found that the manufacturing challenge lies in finding a suitable binder that can withstand the harsh and corrosive conditions that the filters in most cases are subjected to.[11]Within the area of molten aluminum filtration, it is known that the commonly used phosphate-bonded ceramic foam filters are less resistant when filtrating magnesium (Mg) containing alloys. However, the $AlPO_4$ degradation mechanism is not clearly understood, and very little have been reported on the topic in the literature. According to Aubrey *et al.*,[12] X-ray diffraction analysis of phosphate-bonded Al_2O_3-based ceramic foam filters, after immersion testing in an AlMg4.5Mn0.4 melt, confirmed the presence of Mg_3P_2 and MgO in the exposed filters. As a result, Eq. [1] was proposed to have taken place during the trials.

$$3AlPO_4 + 3Mg \rightarrow Mg_3P_2 + 3MgO + AlP. \qquad [1]$$

Solem *et al.*[13] published diagrams with Gibbs free energy as a function of temperature for reactions between a series of common alloying elements in aluminum and 1 mole of phosphorus, which indicated that the formation of AlP is highly favorable at the casting temperature of aluminum. The formation of Mg_3P_2 was, however, not included in those diagrams, but if that had been the case it would have shown that Mg_3P_2 is more favored/stable than AlP at the temperature interval of interest (600 to 800 °C).

Related work has been performed by Doutre,[14] which describes that both AlP and Mg_3P_2 are potential products from reduction of bone ash when in contact with an aluminum-magnesium (Al-Mg) alloy. Bone ash, in which the main constituent is $Ca_3(PO_4)_2$ with small amounts of $CaCO_3$, $Mg_3(PO4)_2$, and CaF_2,[7] is a fine white powder created by the calcination of animal bones and is used on refractory materials in the aluminum industry to prevent molten metal from sticking/reacting with the refractory. Both AlP and Mg_3P_2 could further react with water or moisture in the air according to Eqs. [2] and [3] and form phosphine gas (PH_3).[14] The formation of PH_3 (g) was proved post melt exposure by Aubrey *et al.*, using Dräger tubes and a handheld photoionization detector.[12]

$$Mg_3P_2 + 6H_2O \rightarrow 2PH_{3(g)} + 3Mg(OH)_2 \qquad [2]$$

$$AlP + 3H_2O \rightarrow PH_{3(g)} + Al(OH)_3. \qquad [3]$$

PH_3 (g) is defined as an extremely flammable (F +) and very toxic (T +) gas, which is dangerous for the environment (N).[15] The recommended exposure limits for PH_3 (g) set by the US National Institute for Occupational Safety and Health (NIOSH) are 0.3 ppm for TWA* and 1 ppm for STEL **.[16] In addition, PH_3 (g) has an autoignition temperature of 38 °C,[17] and has been identified as a likely cause for salt cake† landfill fires.[14]

*TWA (Time-Weighted Average) is described as the average exposure over an 8-hour period, i.e., a working day

**STEL (Short-Term Exposure Limit) is described as the average exposure over a period of 15 minutes

†Salt cake is a biproduct from the aluminum industry that normally includes used ceramic foam filters

In 1997, an estimated 800,000 tons of salt cake was annually landfilled in the US,[18] and it has been estimated that salt slags typically can emit around 0.03 to 0.06 m^3 $PH_{3(g)}$ per ton salt cake.[19]

The main objective of the present study has been to investigate the chemical stability of phosphate-bonded Al_2O_3-based ceramic foam filters in contact with molten aluminum, *i.e.,* with pure aluminum and an aluminum-magnesium (Al-Mg) alloy, as well as to measure any subsequent release of PH_3 (g). In addition, thermodynamic calculations have been performed to support the findings.

II. EXPERIMENTAL MATERIALS AND PROCEDURES

A. *Characterization of Aluminum Melts and Ceramic Foam Filters*

All ceramic foam filters were subjected to two different aluminum melts to test the influence of magnesium on their chemical stability, *i.e.* pure aluminum (with traces of magnesium) and an aluminum-magnesium alloy (AlMg2). The AlMg2 alloy was manually prepared from pure aluminum ingots with additions of magnesium to the melt at 740 °C and subsequent stirring for ~ 1 minute. The use of spark optical emission spectroscopy (SOES-ARL 4460, Thermo Fischer Scientific) revealed that there were small variations in the composition of the AlMg2 batches, especially in regard to the Mg concentration (ranging from 2.22 to 2.32 wt pct), see Tables I and II.

Three different Al_2O_3-based ceramic foam filters were tested in two distinct experimental set-ups, see Table III. As can be seen from the table, the majority of the tested filters were of grade 30 except for the 100pctAl_2O_3 filter used during the gravity priming procedure, which was of grade 40 (grade is a newly introduced term explaining functional pore size equal to ppi (pores per inch)). All filters were characterized as received, by embedding samples of the filters in an epoxy resin with subsequent grinding and polishing. The polished samples were investigated with the help of an Ultra 55 LE scanning electron microscope (SEM) (Zeiss, Germany) equipped with an XFlash Detector 4010 energy-dispersive X-ray microanalysis (EDS) unit (Bruker AXS, Germany). The chemical composition of the different filters is also presented in Table III, and is based on 6 measurements from a window size of ~ 10 × 10 μm^2. As can be seen from the table, the Al_2O_3 + P1 and Al_2O_3 + P2 filters were phosphate-bonded ceramic foam filters, whereas the 100pctAl_2O_3 filter was phosphate free and used as a reference. Additionally, mercury intrusion porosimetry (MIP) measurements were performed for evaluation of the size of the pore structures using an Autopore 5 (Micromeritics, USA). A penetrometer (with a cup volume of 15 cm^3 and a stem volume of 0.392 cm^3) was used, which allowed for measurements of relatively large samples (> 10 × 10 × 10 mm^3). A total of 295 measuring points was used, ranging between 0.15 and 420 MPa, with an equilibrium time of 5 seconds. The measured pressure p was converted into the corresponding pore radius r with the help of Washburn's equation (see Eq. [4]) where θ is the contact angle (140° was used) and γ the surface tension of mercury (0.485 Nm^{-1} was used).

$$p = 2\gamma\cos\theta/r. \qquad [4]$$

B. *Priming Procedures*

For the investigation of the chemical stability of ceramic foam filters when in contact with molten

Table I. The Average Chemical Composition of the Main Components in the Aluminum Melts Used During Gravity Priming of Ceramic Foam Filters

Alloy	Si	Fe	Cu	Mn	Mg	Zn	Al
Pure Al	0.07 ± 0.007	0.17 ± 0.005	n/a	n/a	0.0018 ± 3E^{-4}	0.01 ± 1E^{-4}	99.69 ±0.02
AlMg2	0.10 ± 0.02	0.19 ± 0.01	n/a	0.20 ± 0.01	2.33 ± 0.09	n/a	97.11 ±0.1

The chemical compositions were acquired by SOES at the start of each trial and are presented in [Weight Percent]. Very low or not applicable values are stated as n/a.

Table II. The Average Chemical Composition of the Main Components in the Aluminum Melts Used During Electromagnetic Priming of Ceramic Foam Filters

Alloy	Si	Fe	Cu	Mn	Mg	Zn	Al
Pure Al	0.05 ± 6E^{-4}	0.14 ± 0.003	n/a	n/a	0.00035 ± 6E^{-5}	n/a	99.78 ± 0.004
AlMg2	0.06 ± 7E^{-4}	0.17 ± 0.002	n/a	n/a	2.26 ± 0.04	n/a	97.48 ± 0.04

The chemical compositions were acquired by SOES at the start of each trial and are presented in [Weight Percent]. Very low or not applicable values are stated as n/a.

Table III. A Test Matrix Presenting the Different Ceramic Foam Filters

Filter Identification	Electromagnetic Procedure	Gravity Procedure	Composition [Weight Percent]
Al_2O_3 + P1	grade 30	grade 30	Al_2O_3-based, with ~ 4.7 pct P and ~0.6 pct Si
Al_2O_3 + P2	—	grade 30	Al_2O_3-based, with ~ 2.8 pct P, ~ 3.2 pct Si and ~ 0.4 pct Na
100 pctAl_2O_3	grade 30	grade 40	Al_2O_3-based, no other elements identified

aluminum, it is essential to initially prime the filters, *i.e.*, filling the filter's functional porosity with molten metal and removing entrapped air. Priming of filters usually requires a metal head of several cm (lab scale) to create sufficient pressure to initiate a flow of metal through the filter.[20] This implies that a simple dipping of the filters in a molten metal bath will not achieve filling of the functional porosity.

In the present study, two different priming procedures were used, *i.e.*, gravity priming and electromagnetic priming. In the gravity priming procedure, an adequate metal head was secured to achieve metal filling of the functional pores. This priming procedure simulated conventional cast house priming and allowed for dynamic conditions in regard to total immersion time. In the case of the electromagnetic priming procedure, an electromagnetic field was used for filter priming, which also allowed for the measurement of metal composition and PH_3 (g) formation.

1. *Gravity priming*

The gravity priming trials were performed using a customized immersion set-up utilizing a resistance furnace equipped with an automatic temperature control unit and a Noltina Stabil crucible (Morgan MMS, Germany). Four fused silica tubes acting as sample holders for the filters were individually clamped and connected to a rotating wheel. This set-up allowed the tubes to be lowered into the molten metal bath and slowly lifted before being lowered again, to simulate the filtration step where metal flows through the filter, see Figure 2. The clamps were designed in such a way that the silica tubes went through the same reciprocating up-and-down motion in the bath, but could be individually removed from the bath at different times. The furnace was filled with 41 kg of aluminum which was melted and heated up to a temperature of 730 °C (see Table I for details on the chemical composition). Three trials were performed at the same day using the same 41 kg of molten aluminum, but in between each trial 1 to 3 kg of new metal was added to keep the level of the aluminum melt constant and compensate for oxidation of magnesium.

The tested filters had a diameter of 4 cm and a height of 5 cm, and prior to being used they were stored at a temperature comparable to casthouse conditions. They were glued into individual fused silica tubes, which were coated with boron nitride (BN) on the lowermost parts (approximately at the same height as the filters), using an inert Ca-Al-B glass. The four filter tubes were preheated using an air velocity burner to temperatures between 708 °C and 840 °C measured by individual thermocouples placed inside each silica tube. Efforts were made to avoid direct heating of the filters, before they were immersed into the molten aluminum. Prior to lowering the filters into the bath, the aluminum oxide layer on the surface of the molten aluminum was removed from the area of tube immersion. The priming

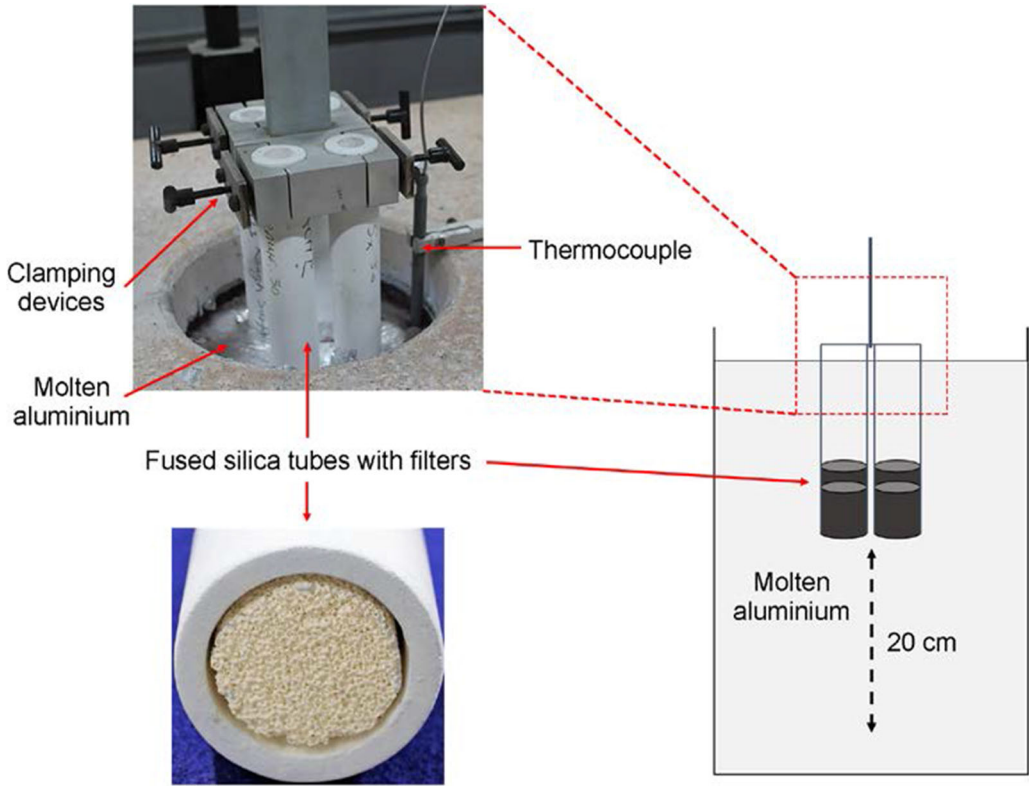

Fig. 2—Set-up of the gravity priming experiments with a reciprocating up-and-down motion of the filters in an aluminum melt.

of the filters was reached by a 20 cm vertical movement of the filter tubes, resulting in a sufficient metal head pressure, melt stirring, and melt movement within the filter. The vertical movement corresponded to an industrial filtration velocity of 14.11 kg/cm^2·hour per filter, which was calculated using the amount of metal passing through the filter per second (0.049 kg/second based on the height and the pace (24.2 seconds per motion) of the filter movement, assuming that the complete filter volume was aluminum) and dividing that by the filter inlet area (12.57 cm^2). The samples tested in the same trial were either removed simultaneously from the bath after 30, 60, 90, and 120 minutes, or one by one at different times. After removal from the bath, the filters were placed on a chill plate to minimize the drainage of the molten metal from the filters, thereby securing as much solidified aluminum within the filters as possible. Further cooling was performed in ambient conditions. All filters were tested using the gravity priming procedure.

2. *Electromagnetic priming*

The electromagnetic priming trials were performed by applying an electromagnetic field around a crucible with molten metal and submerging the filter samples into the melt,[20,21] see Figure 3. As can be seen from the figure, a coil prepared from water-cooled copper tubes in two layers were used for the generation of an electromagnetic field of 80.0 mT in the center of the coil (measured with a Hall Effect gauss meter, model 6010 by Pacific Scientific OECO, F.W. Bell®, USA). The coil was connected to a power supply delivering a voltage of 29 V and a current of 540 A. The experimental set-up is based on patented technology developed at the lab of the Department of Materials Science and Engineering, Norwegian University of Science and Technology (NTNU).[22]

The aluminum metal used during the trials (see Table II for the chemical composition) was melted at 730 °C in a resistance furnace within a boron nitride (BN)-coated Salamander Super A8 crucible (Morgan MMS, Germany). Argon gas (5N), at a flow rate of 2 standard liters per minute (SLPM), was used to reduce melt oxidation. Samples of the molten metal were secured with the help of a scoop prior to filter submersion and at an interval of 30 minutes during the trials, *i.e.,* 5 samples cast in a copper chill mold were retrieved from each trial. The chemical compositions of the samples were obtained by spark optical emission spectroscopy (ARL 4460, Thermo Fischer Scientific, USA). Prior to filter submersion as well as each sampling, the melt surface was skimmed.

The priming procedure was performed by removing the crucible with the molten metal from the furnace and positioning it in the center of the coil with subsequent immersion of a filter, with a size of 5 × 5 × 5 cm^3 and preheated to ~ 600 °C, for 20 to 35 seconds while the magnetic field was applied. Priming was observed to occur almost instantly, and a temperature drop of 22 ± 3 °C was measured as an effect of the priming procedure and the initial sampling. After priming, the crucible was placed back in the furnace for 2 hours

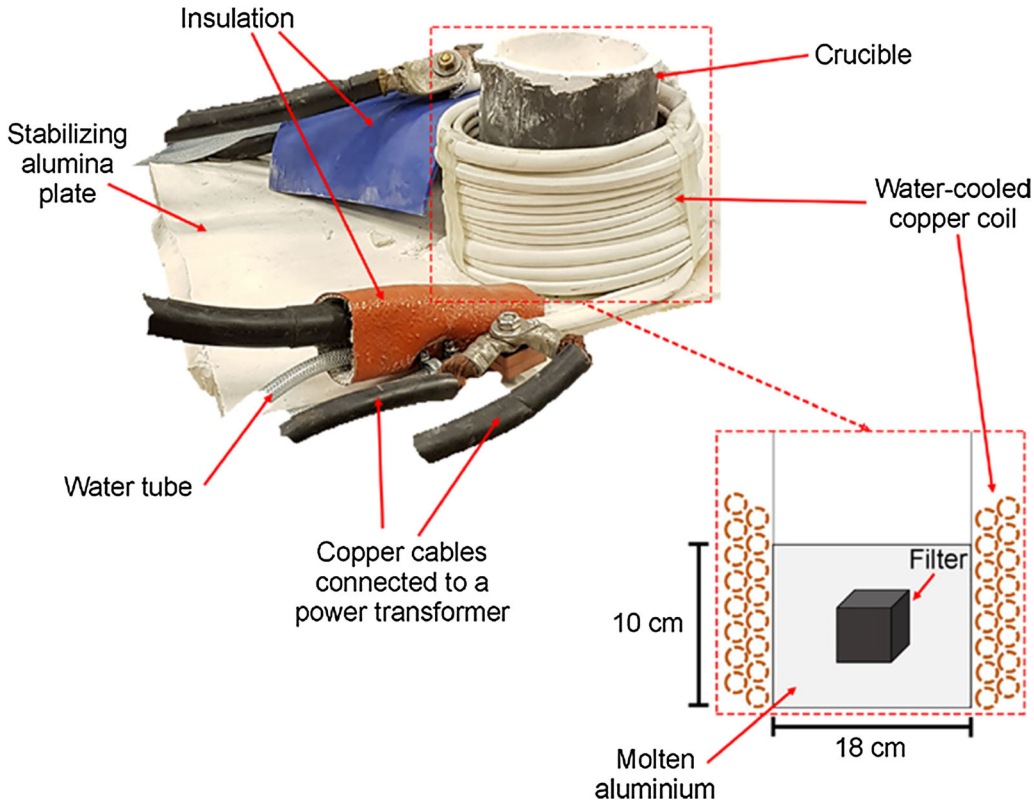

Fig. 3—Set-up of the electromagnetic priming experiments with a two layered copper coil and a crucible with a filter submerged in an aluminum melt (Color figure online).

securing melt reheating. The filter was moved around in the crucible prior to each melt sampling sequence, to obtain a high uniformity of the chemical composition of the sample as well as to induce some melt movement within the filter.

The filter was removed from the aluminum melt at the end of the trial and cooled to room temperature in air with an absolute humidity in the range 7.27 to 9.39 g/m^3 (which is based on historic data from the Norwegian Meteorological Institute[23] and the saturation pressure at different temperatures,[24] with the assumption that the humidity is equal outside and inside). The retrieval step did, however, cause some of the melt to drain from the filter (see Figure 4), which was taken into consideration during sampling. The filter was tested for generation of PH_3 (g) using a Dräger-Tube®[25] positioned ~ 1 cm above the cooling filter, ~ 30 minutes after retrieval. Due to the hazardous nature of PH_3 (g), strict safety measures were taken upon filter handling and gas measuring, *i.e.*, gas mask, gas safety detector, room ventilation, and filter sample storage in a ventilated cabinet post handling.

C. *Sample Preparation and Analyzing Methods*

A sample with the dimensions ~ 30 × 30 mm^2 was secured from each gravity primed filter, and with the dimensions ~ 15 × 15 mm^2 from each electromagnetically primed filter. The samples were cut from the bottom of each filter, at the same position each time (see Figure 4), and mounted in epoxy with subsequent grinding using SiC paper down to a size of 5 μm, with either water or ethanol as lubricant.

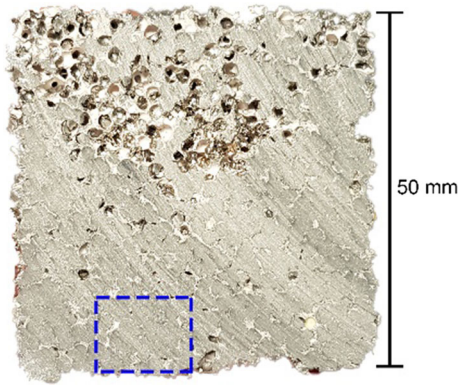

Fig. 4—Position (blue dotted square) of the sample secured from each filter tested using both the gravity- and electromagnetic priming procedures (the present filter is electromagnetically primed) (Color figure online).

The samples were analyzed by light optical microscopy (LOM) using a Leica MEF4M (Germany) unit connected to the ProgRes CapturePro software system (Jenoptik, Germany). Polarized light and a teal colored filter were used to visualize and increase the contrast between the filter media, the metal phase, and the interface between the two. Each sample was analyzed at

magnifications ranging from 25× to 200×. Qualitative chemical analyses of the same areas were later performed by electron probe microanalysis (EPMA) using a JEOL JXA-8500F (Germany) unit. The analysis was performed on an area of $1 \times 1\ mm^2$ with a probe current of 30 nA for the mapping of the elements Al, O, P, C, Si, Mg, Ti, Fe, K, and B. Analysis was also performed by field emission scanning electron microscopy (FESEM) using a Zeiss Ultra 55 Limited Edition (Germany) unit with an accelerating voltage of 10 kV and a working distance of 10 mm. The chemical composition of the cast metal samples was analyzed by spark optical emission spectroscopy (SOES) using an ARL 4460 (Thermo Fischer Scientific, USA) unit.

In addition, one sample immersed in pure aluminum was examined with the help of transmission electron microscopy (TEM). A thin lamella was collected from the filter–metal interface with a focused ion beam scanning electron microscope (FIB-SEM) using a Helios G4 UX Dual-beam (Thermo Fisher Scientific, USA) unit. The lamella was cut out from the sample and transferred to a dedicated copper half grid using a standard lift-out technique. Coarse thinning was performed at an acceleration voltage of Ga+ ions of 30 kV, while the final thinning was performed at 5 and 2 kV to minimize surface damage on either side of the lamella. Element analysis was performed with a double Cs aberration-corrected cold field emission gun (FEG) using a JEOL ARM 200FC (Japan) unit equipped with an energy-dispersive X-ray microanalysis (EDS) detector (Centurio, JEOL, Japan) and a dual electron energy loss spectrometer (EELS) unit (Quantum ER GIF, Gatan, USA). The FEG was operated at 200 kV.

III. RESULTS AND DISCUSSION

A. *Thermodynamics*

The Gibbs free energy (ΔG) as a function of temperature has been plotted for the reactions presented in Eqs. [2] and [3] with data from the Reaction Equations module of HSC Chemistry® 9.9.2.3, see Figure 5. As can be seen from the figure, the driving force for the formation of PH_3 (g) from both AlP and Mg_3P_2 is negative when the species are in contact with sufficient quantities of H_2O. Thus, both species will spontaneously form PH_3 (g) when in direct contact with either water or the moisture in the air. However, for these reactions to actually take place AlP and Mg_3P_2 will have to be present in the system.

Table IV. Equilibrium Calculations of the Output Mass of AlP and $MgAl_2O_4$ When an Al-Mg Melt Comes in Contact with a Phosphate-Bonded Al_2O_3-Based Ceramic Foam Filter at 730 °C and 1 atm Pressure (the Filter Constituents Were Added as Components in the Melt)

Species	Input Mass [g]	Output Mass [g]
Al	2200	—
Mg	55	—
Al_2O_3	45	—
$AlPO_4$	5	—
AlP	—	2
Spinel (78 wt pct $MgAl_2O_4$)	—	54

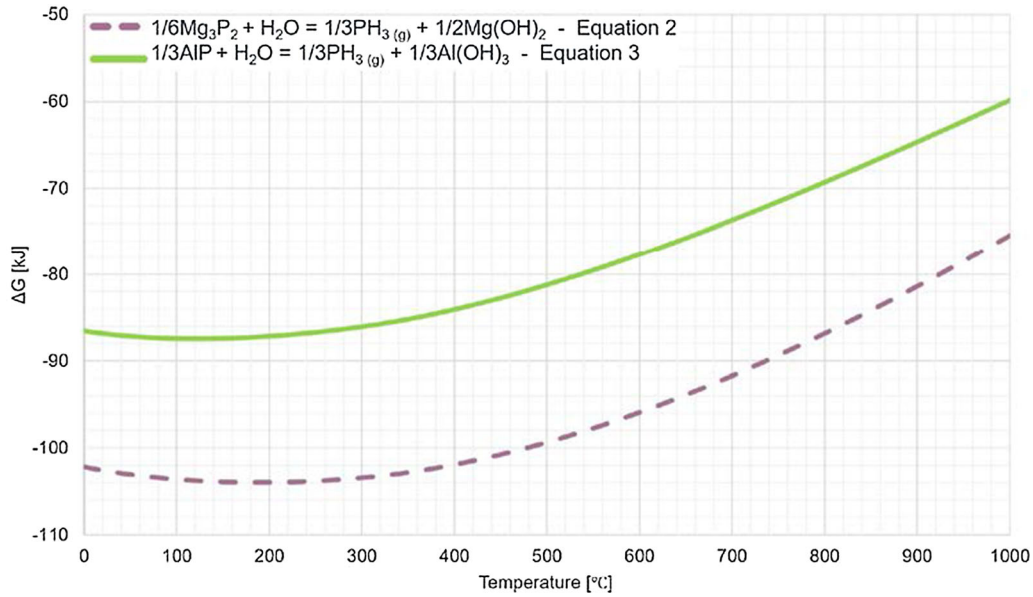

Fig. 5—Gibbs free energy (ΔG) as a function of temperature for reactions where the species AlP and Mg_3P_2 react with 1 mole of H_2O, in the temperature range of 0 to 1000 °C, drawn using data from the Reaction Equations module of HSC Chemistry® 9.9.2.3.

The amounts of AlP and $MgAl_2O_4$ produced when an Al-Mg melt comes in contact with a phosphate-bonded Al_2O_3-based ceramic foam filter at 730 °C and 1 atm pressure have been calculated in an open system with a protective atmosphere of Ar (g), see Table IV. The Equilib module in the FactSage™ 7.3 software was used for the calculation together with the FactPS, FToxid, and FTlite databases. The input values were based on the experimental conditions used in the present study during electromagnetic priming of a 50 g Al_2O_3-based filter (assumed to contain 5 wt pct of an $AlPO_4$ binder [5]), in a Mg-alloyed aluminum melt (2.5 wt pct Mg given zero Mg oxidation). Moreover, the calculation was performed in an open system over 100 steps with 2 liters of Ar (g) added at each step and ~ 0.6 liters of air with a water vapor content of ~ 30 pct at step 1 (N_2 in the air was treated as inert). It was assumed that equilibrium existed between all phases at all times, and the reaction kinetics was neglected. In addition, the filter constituents were added as components in the melt. The change in conditions over the steps, as well as the output mass of each component, proved to be insignificant.

As can be seen from Table IV, formation of AlP and $MgAl_2O_4$ will occur for the evaluated case, hence also under normal aluminum cast house conditions. In other words, some of the P released from the $AlPO_4$ binder will form AlP, while the rest will enter the aluminum melt (will be discussed in more detail later).

A predominance diagram for the system Al-Mg-P-O, assumed to consist of an ideal gas mixture of O_2 (g) and P_2 (g), was also calculated at a fixed temperature of 727 °C using the Predom module of the FactSage™ 7.3 software and the same databases as in previous calculations, see Figure 6. The area on the right side of the diagram representing the area for Al_2O_3 (s) and $MgAl_2O_4$ (s) extends to a partial pressure of O_2 (g) equal to 1×10^{-23} atm and more or less the complete interval of the partial pressure of P_2 (g). As a result, the line on the left side of this area (marked with a pink dotted line) represents the boundary layer between the filter medium and the bulk of the aluminum melt. The partial pressures of O_2 (g) and P_2 (g) were also calculated using the same case as above, *i.e.*, the electromagnetic priming conditions, resulting in values equal to 6.3×10^{-49} and 7.6×10^{-16} atm, respectively. As can be seen from the diagram, the phases that will form at these partial pressures are AlP (s) and $MgAl_2O_4$ (s) (marked with a red dot and red lines). The diagram also reveals that small changes in the partial pressures will affect phase formation.

B. *Characterization of Unexposed Filters*

The porosity of the different filter materials (as received) was investigated by the use of scanning electron microscopy, and clear differences were identified to exist, see Figure 7. As can be seen from the figure,

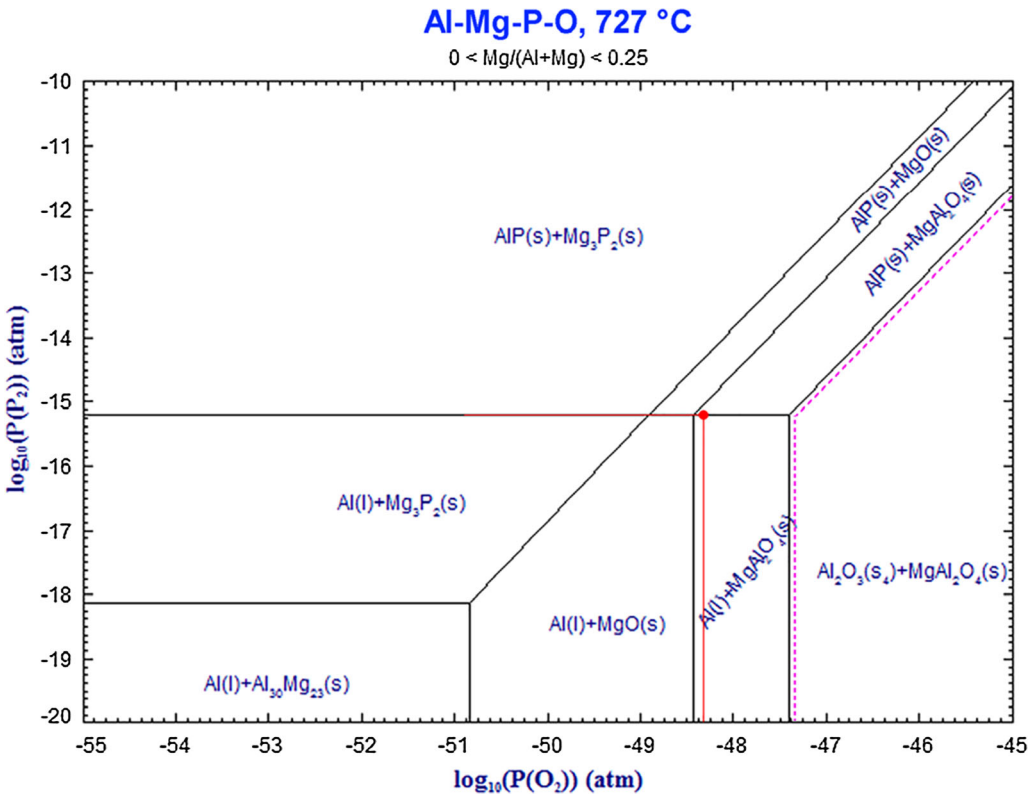

Fig. 6—A predominance diagram for the system Al-Mg-P-O at 727 °C, as calculated by FactSage™ 7.3, with the logarithm of the partial pressures of O_2 (g) and P_2 (g) on the x- and y-axis, respectively. The pink dotted line represents the boundary layer between the filter medium and the bulk of the aluminum melt, and the red dot and lines mark the calculated partial pressures for O_2 (g) and P_2 (g) during electromagnetic priming of a phosphate-bonded Al_2O_3-based ceramic foam filter in an Al-Mg melt (Color figure online).

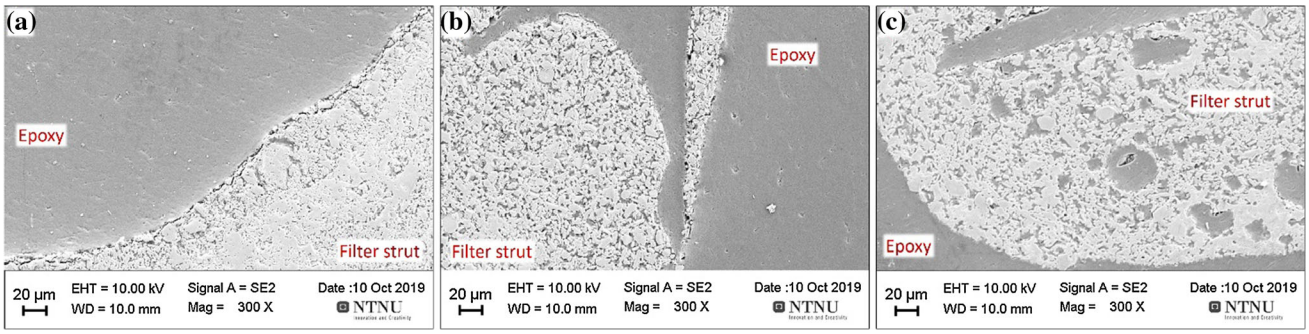

Fig. 7—SEM micrographs of the following as-received filters: (*a*) 100pctAl_2O_3, (*b*) Al_2O_3 + P1, and (*c*) Al_2O_3 + P2.

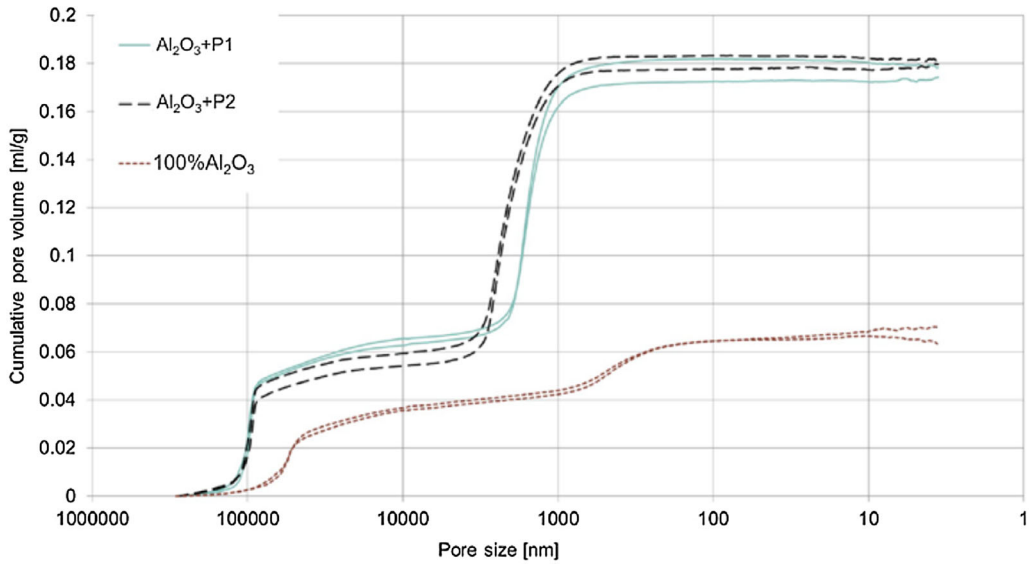

Fig. 8—Cumulative pore volume as a function of the pore size measured by mercury intrusion porosimetry (MIP).

the 100pctAl_2O_3 ceramic foam showed a relative dense microstructure of the struts compared to the commercial Al_2O_3 + P1 and Al_2O_3 + P2 foams. The latter even consisted of a significantly larger pore size than Al_2O_3 + P1.

The differences in porosity between the foams were measured by mercury intrusion porosimetry giving the following results: ~ 20 pct for 100pctAl_2O_3, ~ 37 pct for Al_2O_3 + P1 and ~ 41 pct for Al_2O_3 + P2. The cumulative pore volumes as a function of the pore size were plotted for each of the performed measurements, see Figure 8. As can be seen from the figure, a two-step increase of the cumulative pore volume can be identified. The first strong increase, where the pore sizes of the Al_2O_3 + P1 and Al_2O_3 + P2 filters were measured to be ~ 100 μm and for 100pctAl_2O_3 ~ 60 μm, corresponds to the filling of mercury in the strut cavities of the foam.[26] The variations between the phosphate-bonded Al_2O_3 and the pure Al_2O_3 filters are believed to be the result of differences in the polyurethane foam used during production, as well as in the ceramic composition (as the 100pctAl_2O_3 filter shrunk during sintering which was not the case for the phosphate-bonded Al_2O_3 + P1 and Al_2O_3 + P2 filters).

The second strong increase of the cumulative mercury volume occurred at mean pore sizes of ~ 1.5 μm for the Al_2O_3 + P1 filter, ~ 2.2 μm for the Al_2O_3 + P2 filter, and ~ 0.4 μm for the 100pctAl_2O_3 filter, corresponding to the filling of the pores in the strut, *i.e.*, the material porosity. The small mean pore size of the 100pctAl_2O_3 foam confirms the observation made by scanning electron microscopy.

The difference in pore size measured with scanning electron microscopy and mercury intrusion porosimetry can be explained by a difference in the measuring techniques. During mercury intrusion porosimetry, the pores in the interior of the sample can only be reached by mercury through a chain of entryways between the pores. As a result, the larger pores in the strut center are not intruded by mercury before the pressure needed to penetrate the narrower entryways is reached. Thus, the mercury intrusion porosimeter

measures the largest entrance of a pore and not the pore cavities themselves. In contrast, scanning electron microscopy images allow the observation of the pore cavities.

The chemical composition of the ceramic foam filters was characterized using energy-dispersive X-ray microanalysis and revealed, as previously presented in Table III, that $Al_2O_3 + P1$ and $Al_2O_3 + P2$ were phosphate-bonded filters whereas the $100pctAl_2O_3$ was phosphate free.

C. *Gravity Priming*

Light optical microscopy images of the three different filters immersed by gravity priming for 120 minutes in pure aluminum and AlMg2 are presented in Figures 9 and 10. The turquoise color seen in the images is, as previously mentioned, the result of using a teal colored filter to compensate for optical and illumination issues in order to improve contrast.

No visual degradation could be observed in either of the filters immersed in the pure aluminum melt (see Figures 9(a) through (c)) or in the case of the $100pctAl_2O_3$ filter immersed in the AlMg2 melt (see Figure 10(a)). A clear color change from milky white to different gradients/shades of brown/black was, however, visible at the edge of the $Al_2O_3 + P1$ filter immersed in AlMg2, see Figure 10(b). As can be seen from this image, a layered gradient exists from the filter–metal interface to the center of the filter strut, *i.e.,* from a darker brown/black area at the filter–metal interface and ~ 100 μm inwards (marked with 4), succeeded by a ~ 50μm lighter brown area (marked with 5), followed by an unreacted milky white area at the center of the strut (marked with 6). These changes in color indicate that a reaction and/or self-diffusion of elements to or from the filter have occurred. The $Al_2O_3 + P2$ filter, see Figure 10(c), revealed a more uniform brown/black color throughout, indicating that the changes in question had occurred throughout the whole filter strut.

Elemental mapping of the filters immersed in AlMg2 was performed by electron probe microanalysis, where the elements Al, O, P, C, Si, Mg, Ti, Fe, K, and B were analyzed. Only the most interesting results for the present study are presented, *i.e.*, the results of Al, O, P, and Mg. As can be seen from Figure 11, the $100pctAl_2O_3$ filter reveals the presence of Al and O with only a minor intrusion of Mg into the strut. No further reactions seem to have taken place.

A stepwise (layer by layer) increase of the concentration of P from the edge of the filter towards the center of the strut can be seen from the elemental mapping of the $Al_2O_3 + P1$ filter presented in Figure 12, with the lowest concentration of P at the filter–metal interface, *i.e.*, at

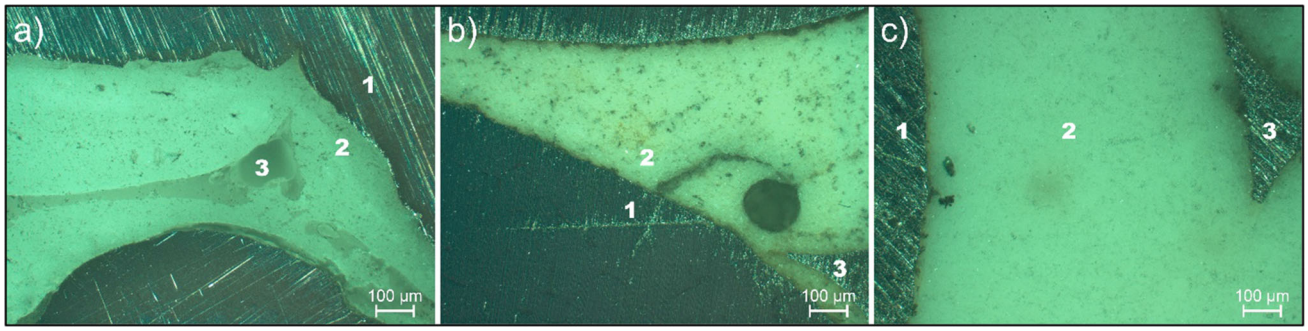

Fig. 9—LOM images at 100x magnification of the filters immersed with gravity priming for 120 min in pure aluminum: (*a*) $100pctAl_2O_3$, (*b*) $Al_2O_3 + P1$, and (*c*) $Al_2O_3 + P2$. Polarized light and a teal color filter were used, which explains the turquoise color. The numbers in the images mark the following phases: (1) aluminum, (2) filter strut, and (3) strut cavity (Color figure online).

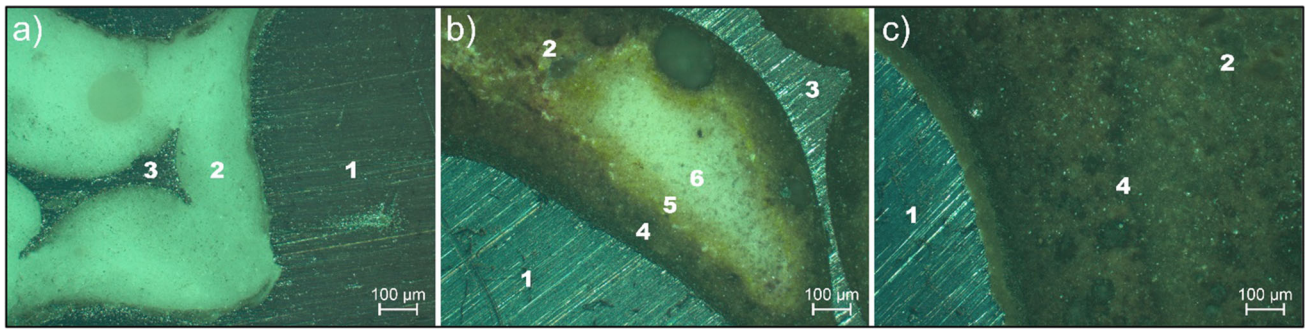

Fig. 10—LOM images at 100x magnification of the filters immersed with gravity priming for 120 min in AlMg2: (*a*) $100pctAl_2O_3$, (*b*) $Al_2O_3 + P1$, and (*c*) $Al_2O_3 + P2$. Polarized light and a teal color filter were used, which explains the turquoise color. The numbers in the images mark the following phases/medias: (1) aluminum, (2) filter strut, (3) strut cavity filled with aluminum, (4) fully reacted area, (5) moderately reacted area, and (6) slightly reacted area (Color figure online).

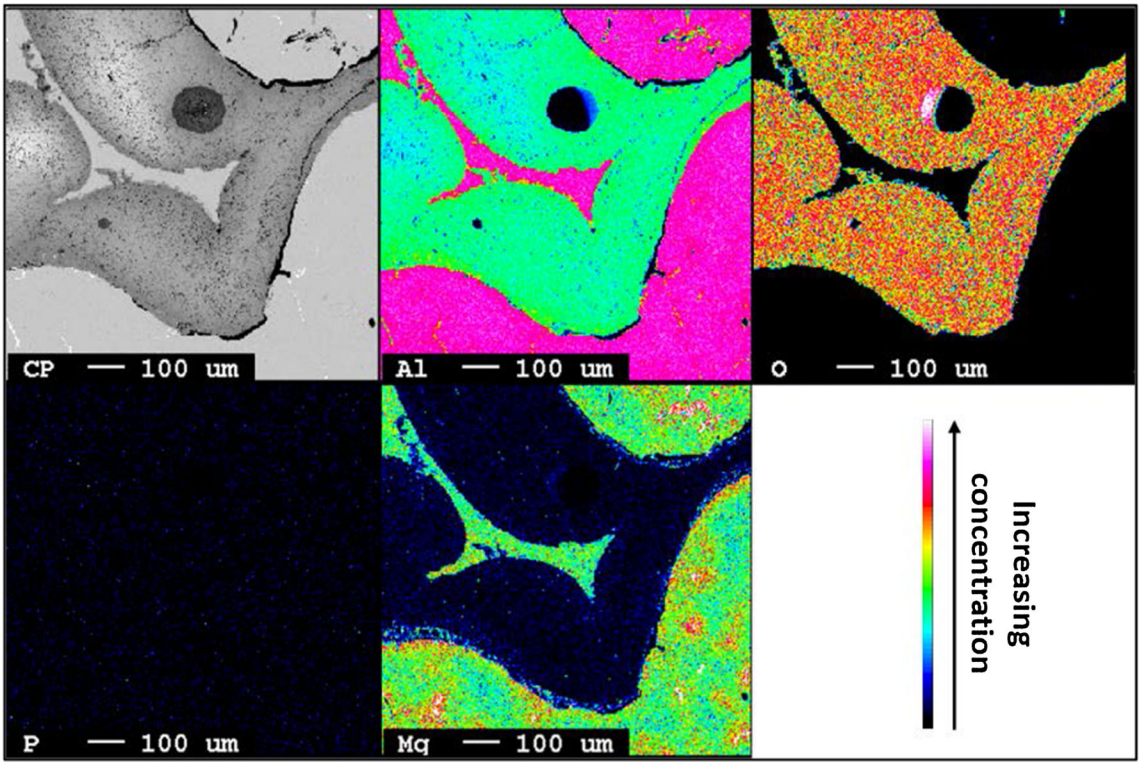

Fig. 11—EPMA mapping of Al, O, P, and Mg for the 100pctAl_2O_3 filter immersed by the gravity priming procedure in the AlMg2 melt for 120 min.

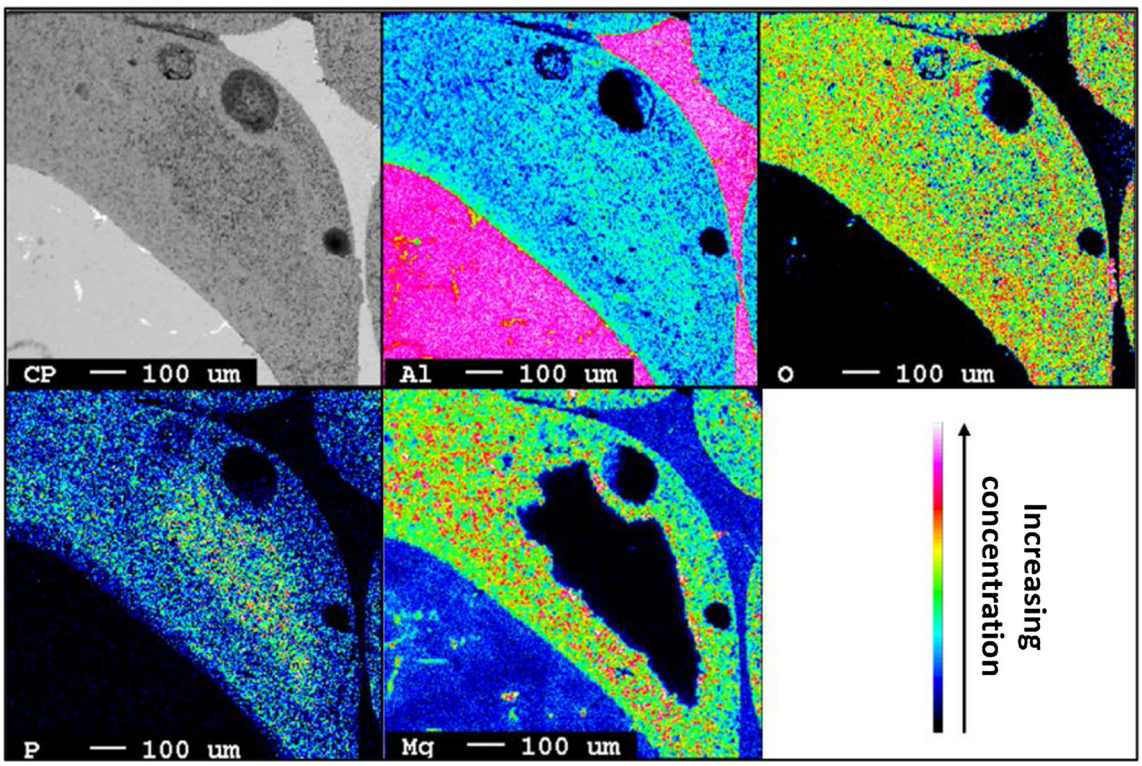

Fig. 12—EPMA mapping of Al, O, P, and Mg for the Al_2O_3 + P1 filter immersed by the gravity priming procedure in the AlMg2 melt for 120 min.

the edge towards the functional pore and the strut cavity. This corresponds well with the discoloration identified by light optical microscopy (Figure 10(b)) if assuming that the discoloration is a result of AlP formation and that some of the P has diffused from the filter into the metal leaving this area of the filter more or less depleted of P. In addition, an increase of the Al and the Mg concentrations was established to exist at the edge of the filter. In the case of Mg, this was the result of diffusion of Mg from the AlMg2 melt into the filter. It is, however, notable that the diffusion at the edge of the strut cavity was at a slightly lower level than at the edge of the functional pore size. The increase of the Al concentration at the edge of the filter strut was less pronounced than the Mg increase, and at the edge of the strut cavity the increase was neglectable (nearly not visible).

In Figure 13(a), a scanning electron microscopy image of the Al_2O_3+P1 filter is presented. It can clearly be seen that metal has penetrated the strut cavities, as well as the material pores within the strut. It is believed that the diffusion of P from the strut edge of the filter into the metal has left pores and/or pore entryways facilitating this penetration and thereby compromising the filter structure. The presence of molten aluminum in the strut cavities has caused a larger reaction area, which in turn has increased the reaction. In Figure 13(b), it can be seen that large fragments of the ceramic structure detached from the filter strut as a result of what is believed to have been an intergranular attack due to binder degradation. Loose filter fragments may cause a reduction of the filter strength and end up in the Al melt, contaminating it and possibly also the final cast product. Even another mechanism has been reported in the literature to enable this process in industrial settings, *i.e.*, lateral compressive edge crushing, which is described as a combination of binder degradation, thermal expansion, and compressive modulus, as well as the lateral compressive stress that the filter is exposed to in the filter bowl.[12]

Elemental mapping of the Al_2O_3+P2 filter revealed a stepwise (layer by layer) change in the concentration of P as well, from the edge of the filter towards the center of the strut, see Figure 14. In this case, the layer at the edge of the strut proved to have the highest concentration of P with a decrease towards the center (which is in contrast to the observations made for the Al_2O_3+P1 filter). As the discoloration identified by light optical microscopy (Figure 10(c)) was more uniform brown/black, the degradation of the binder was believed to have come closer to equilibrium in view of the formation of AlP (again assuming that the discoloration is a result of AlP formation). The higher concentration of P at the edge of the strut is believed to be unreacted P that has diffused from the center of the strut towards the edge for further diffusion into the metal (which has not yet occurred). Moreover, a homogenous distribution of Al throughout the filter was established, and the diffusion of Mg from the AlMg2 melt into the filter was less pronounced with the highest concentration towards the edge of the strut. A gap filled with epoxy, believed to be the result of solidification shrinkage, was also identified to exist at the filter–metal interface containing small amounts of P.

Moreover, metal pore penetration was confirmed by scanning electron microscopy in the case of the Al_2O_3+P2 filter, although at a lesser extent than described for the Al_2O_3+P1 filter. The obtained structure bear close resemblance to observations reported in the literature to be the result of intergranular attacks due to binder degradation.[12]

As the experimental set-up used during the gravity priming trials allowed for the filter samples to be simultaneously immersed into the Al melt but individually withdrawn, trials were also performed varying the immersion time. Light optical microscopy images of the Al_2O_3+P1 and Al_2O_3+P2 filters immersed in AlMg2 for 30, 60, and 120 minutes are presented in Figure 15. As can be seen from Figures 15(a) through (c), a relatively thin discolored layer (dark brown/black) was established to have formed at the edge of the Al_2O_3+P1

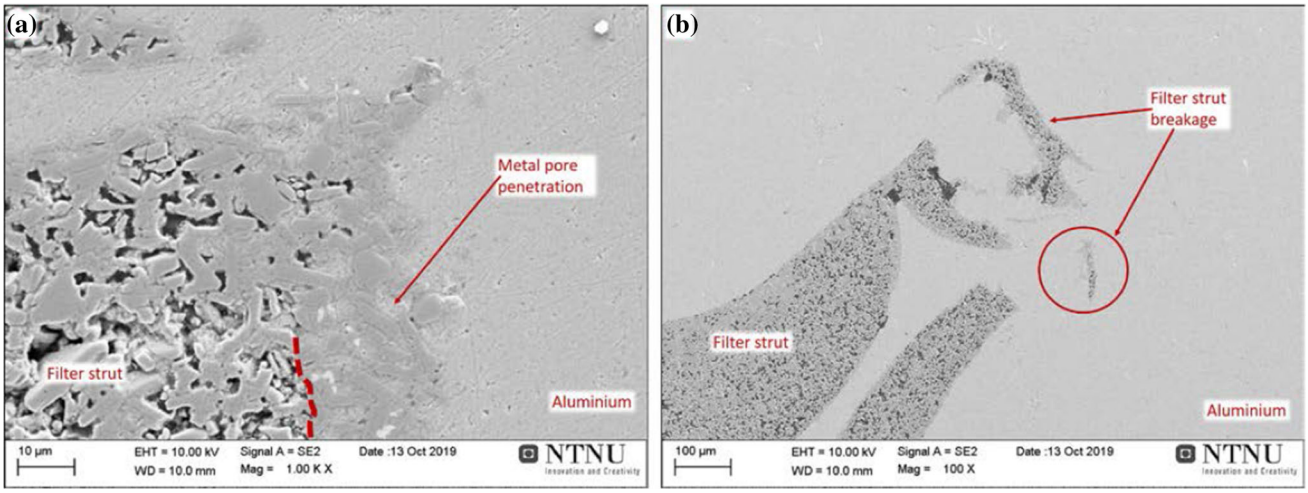

Fig. 13—SEM micrographs of the Al_2O_3+P1 filter immersed by the gravity priming procedure in the AlMg2 melt for 120 min. (*a*) Metal penetration into the strut cavities and material pores within the strut, and (*b*) filter strut breakage.

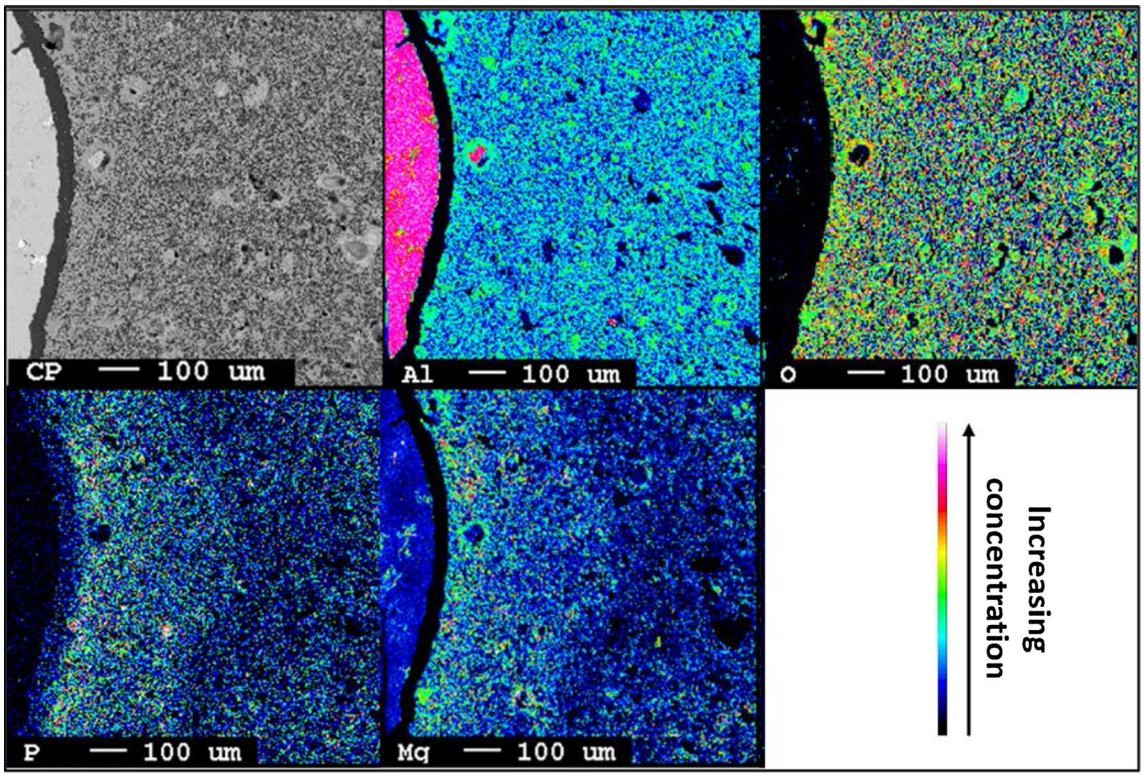

Fig. 14—EPMA mapping of Al, O, P, and Mg for the $Al_2O_3 + P2$ filter immersed by the gravity priming procedure in the AlMg2 melt for 120 min.

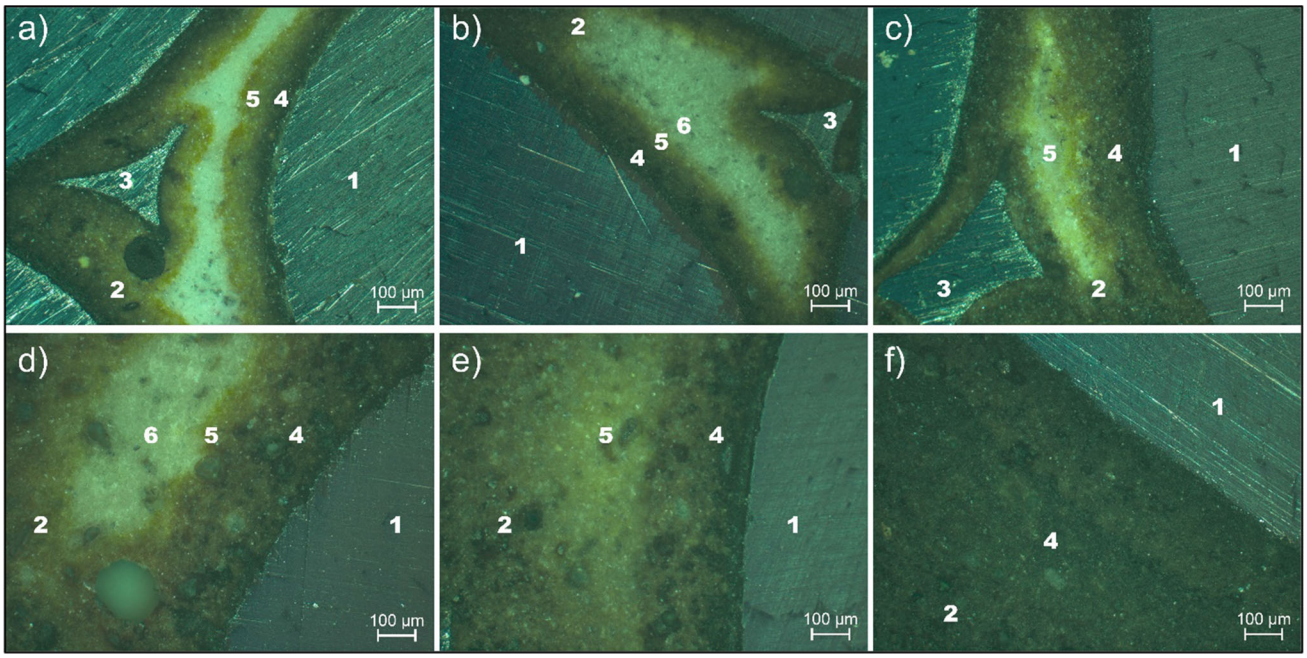

Fig. 15—LOM images at 100× magnification of $Al_2O_3 + P1$ ((*a*) through (*c*)) and $Al_2O_3 + P2$ ((*d*) through (*f*)) filters immersed by the gravity priming procedure in an AlMg2 melt for 30 min ((a) and (d)), 60 min ((*b*) and (*e*)), and 120 min ((c) and (f)). Polarized light and a teal color filter were used, which explains the turquoise color. The numbers in the images mark the following phases/medias: (1) aluminum, (2) filter strut, (3) strut cavity filled with aluminum, (4) fully reacted area, (5) moderately reacted area, and (6) slightly reacted area (Color figure online).

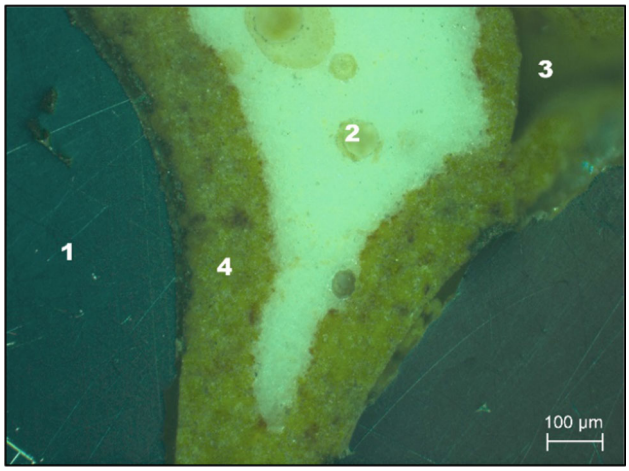

Fig. 16—LOM image at 100× magnification of the Al_2O_3 + P1 filter immersed with electromagnetic priming for 120 min in the AlMg2 melt. Polarized light and a teal color filter were used, which explains the turquoise color. The numbers in the image marks the following phases/medias: (1) aluminum, (2) filter strut, (3) strut cavity (empty), and (4) moderately reacted area (Color figure online).

filter after 30 minutes, increasing in thickness as a function of time. In the case of the Al_2O_3 + P2 filter (Figure 15(d) through (f)), the degradation of the binder seems to have progressed faster, and a thicker discolored layer was established to have formed at the edge of the filter already after 30 minutes. A completely reacted filter was the result after 120 minutes of immersion.

Based on the results from light optical microscopy, electron probe microanalysis, and scanning electron microscopy, it is clear that both phosphate-bonded filters (Al_2O_3 + P1 and Al_2O_3 + P2) have reacted with the AlMg2 melt, affecting the strength of the ceramic structure as a result of binder degradation. It should, however, be noted that the majority of the presented results are images or micrographs, which have the drawback of being methods that opens for subjective analysis. Additionally, filter struts are 3D structures and the plane in which the filter sample is cut can vary between the presented figures, thus potentially affecting the interpretation of the analysis. The advantage, on the other hand, is that all trials within each experimental procedure have been performed in the same manner.

D. *Electromagnetic Priming*

Trials with the Al_2O_3 + P1 and 100pctAl_2O_3 filters immersed in pure aluminum and AlMg2 for 120 minutes were also performed using the electromagnetic priming procedure (a relatively new and innovative procedure allowing the filling of ceramic foam filters with small functional pore sizes without a high metal pressure head [20]). The procedure has the advantages of a low ratio of metal to filter volume, as well as easy access to the aluminum melt during the trial. In other words, samples from the melt that have been in contact with the filter can be collected for further analysis of compositional changes as a result of the filter–metal contact.

Even in this case, no visual degradation could be observed by light optical microscopy in either of the filters immersed in pure aluminum or in the case of the 100pctAl_2O_3 filter immersed in AlMg2. A clear and well-defined color change from milky white to light brown was, however, defined to exist at the edge of the Al_2O_3 + P1 filter and towards the center of the filter strut when immersed in AlMg2, see Figure 16. Following the same pattern as in the gravity priming trials, elements were established to diffuse to and from the filter during immersion in the aluminum melts. The strut cavities were, however, observed to be empty and the filter strut appeared to be less reacted. This is believed to be a direct result of the difference in metal head above the filter needed to initiate priming in the case of the gravity- and electromagnetic procedures, respectively, as well as the lack of molten metal movement within the filter in the case of the electromagnetic procedure.

The chemical composition of the molten metal samples collected during the trials were later analyzed together with samples collected before filter priming, as well as samples from reference trials performed without any filter. For the pure aluminum and the AlMg2 trials, one sample was collected every 30 minutes, and with a total of 12 trials 60 metal samples were analyzed.

The concentrations of P and Mg in the metal samples, *i.e.*, in the samples taken before, during and after the immersion trials, are presented together with the average values and standard deviations for each data set in Figures 17 and 18, respectively. As can be seen from the figures, only minor changes in the concentrations of P and Mg were established to exist for the metal samples secured from the trials with the 100pctAl_2O_3 filters immersed in pure aluminum and in AlMg2. This was also the case for the reference trials. In contrast, the metal samples from the trials with the Al_2O_3 + P1 filters in AlMg2 showed a significant increase of the P concentration from ~ 0.0005 to ~ 0.004 wt pct, as well as a decrease of the Mg concentration from ~ 2.3 to ~ 2.0 wt pct. The large standard deviations obtained for the Al_2O_3 + P1 filters, see Figure 18, are believed to be due to the difference in the initial concentration of Mg in the melt between the trials. It should further be noted that the corresponding results for the trials in pure aluminum was omitted from the figure to ensure graph readability. Unexpectedly, a significant increase in the P concentration also existed for the Al_2O_3 + P1 filters immersed in pure aluminum, *i.e.*, from ~ 0.0005 to ~ 0.0015 wt pct. This is believed to be the result of the initial Mg concentration (0.00035 wt pct as a contaminant) in the pure aluminum, which in turn allowed for a reaction between the filter and the molten metal to take place. P is considered an impurity in aluminum, and even very low amounts would decrease the corrosion resistance and increase the brittleness of the cast metal.[27] It has also been reported that P negatively affects both the formation of eutectic silicon and the eutectic modification using strontium.[28]

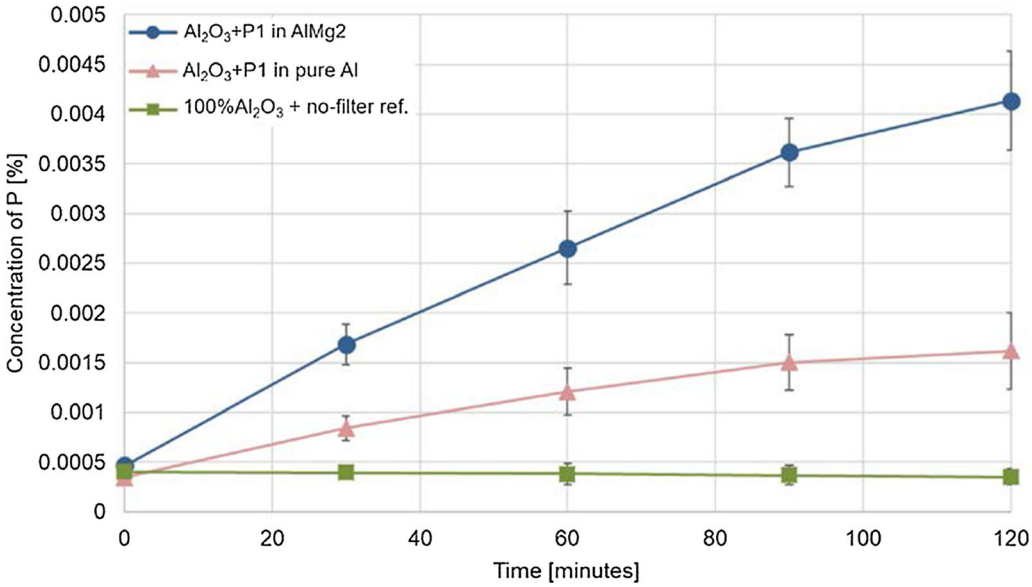

Fig. 17—Concentration of phosphorus (P) in the melt (measured through SOES analysis) as a function of the time the filters were immersed in the molten aluminum. Points are given as an average with standard deviations.

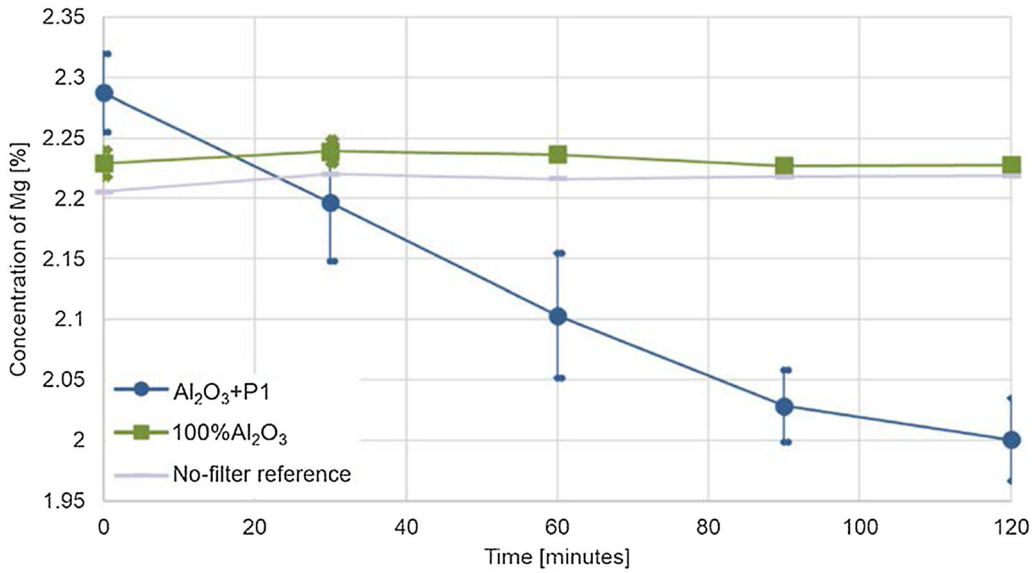

Fig. 18—Concentration of magnesium (Mg) in the melt (measured through SOES analysis) as a function of the time the filters were immersed in the molten aluminum. Points are given as an average with standard deviations.

E. *Release of PH_3 Gas*

During the electromagnetic priming trials, the amount of PH_3 released from the filters immersed in molten metal was measured for each combination of filter and aluminum melt. The filters were allowed to cool for 30 minutes in air at room temperature before the measurement of released PH_3 was performed using a Dräger-Tube® with a measuring sensitivity of 0.1 to 3 ppm. If the first test tube indicated concentrations above 3 ppm, a Dräger-Tube® with a sensitivity of 1 to 100 ppm was used. In each case, the tube was placed just above the filter and held there for 3 minutes or 9 minutes, respectively, depending on the measuring sensitivity of the tube. It should be noted that during the cooling step the filters were only exposed to the

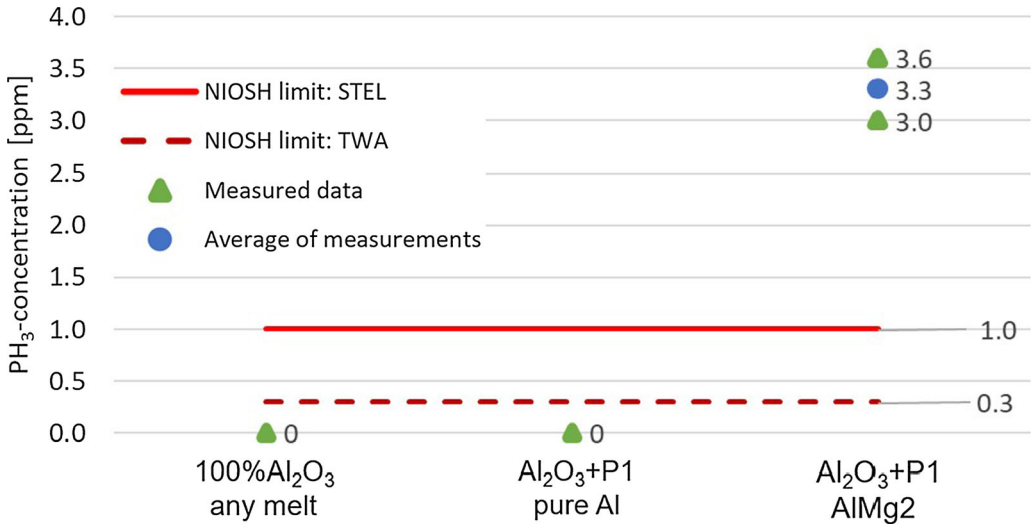

Fig. 19—Measured concentrations of PH_3 gas released from spent filters after cooling in air at room temperature for 30 min, plotted together with the NIOSH's recommended exposure limits.[16]

humidity in the air, where the absolute humidity was in the range of 7.27 to 9.39 g/m^3, which should be similar to what most spent filters are exposed to in an industrial casthouse.

The amount of PH_3 released from the spent filters is presented in Figure 19, together with the National Institute for Occupational Safety and Health's (NIOSH) recommended exposure limits (TWA[‡] and STEL[§]).[16] As can be seen from the figure, no release of PH_3 was measured for the Al_2O_3 + P1 and 100pctAl_2O_3 filters immersed in pure aluminum. However, in the case of the Al_2O_3+P1 filter immersed in AlMg2 the measured average concentration of released PH_3 was 3.3 ppm. This value clearly exceeds the recommended exposure limits of both TWA[4] and STEL[5].[16] Considering that this concentration was measured from a 5 × 5 × 5 cm^3 filter sample while the standard filters used in casthouses today are much larger (typically 60 × 60 × 5 cm^3) is concerning. Despite the mentioned hazardous[15] and flammable[17] nature of PH_3 gas, the actual effect of an Al_2O_3+P1 filter on Health, Safety and Environment in a casthouse has not been documented.

[‡]TWA (Time-Weighted Average) is described as the average exposure over an 8-hour period, i.e., a working day

[§]STEL (Short-Term Exposure Limit) is described as the average exposure over a period of 15 minutes

F. *Investigation by Transmission Electron Microscopy*

Due to the fact that a clear increase of the P concentration was established to exist in the molten aluminum samples from the electromagnetic priming trials with Al_2O_3 + P1 filters immersed in pure aluminum, it was decided to look further into possible explanations. As previously mentioned, the pure aluminum that was used in that case contained very small amounts of Mg as a contaminant (0.00035 wt pct), and the overall effect of Mg on the degradation of the $AlPO_4$ binder phase was therefore believed to be important to understand.

One of the Al_2O_3 + P1 filter samples immersed in pure aluminum for 120 minutes during the gravity priming trials was therefore analyzed by transmission electron microscopy, see Figure 20. As can be seen from this cross section from the bulk of the sample, visible changes in the binder phase were observed. Energy-dispersive X-ray microanalysis of the chemical composition of unaffected and affected areas were performed, *i.e.*, on the binder phase between the Al_2O_3 grains (phase 1) which showed either a homogeneous light gray appearance (phase 2) or an inhomogeneous dark gray appearance (phase 3), in which the latter was assumed to be the phosphate binder after it had reacted with Mg. The obtained results for phases 2 and 3, acquired from an area of 0.3 × 0.3 μm^2, are presented in Table V. However, due to the limited precision of the EDS measurements, the tabulated results must be handled with caution.

As displayed in Table V, the unmodified binder (phase 2) consisted of Al, O, and P as expected, where the ratio quite accurately describes the binder to be $AlPO_4$. The reacted binder (phase 3), however, was measured to maintain the same ratio of Al and O, but with a decreased concentration of P. Furthermore, Mg was detected in this phase, which proves that the diffusion of Mg from the melt to the filter had been very strong even if the Mg concentration of the melt was only 0.0016 wt pct (measured by SOES). Furthermore, the established sharp decrease of the P concentration between phases 2 and 3 indicates that P has diffused from the filter into the melt. This could in turn explain the increase in concentration of P observed in the melt during the electromagnetic priming trials with an

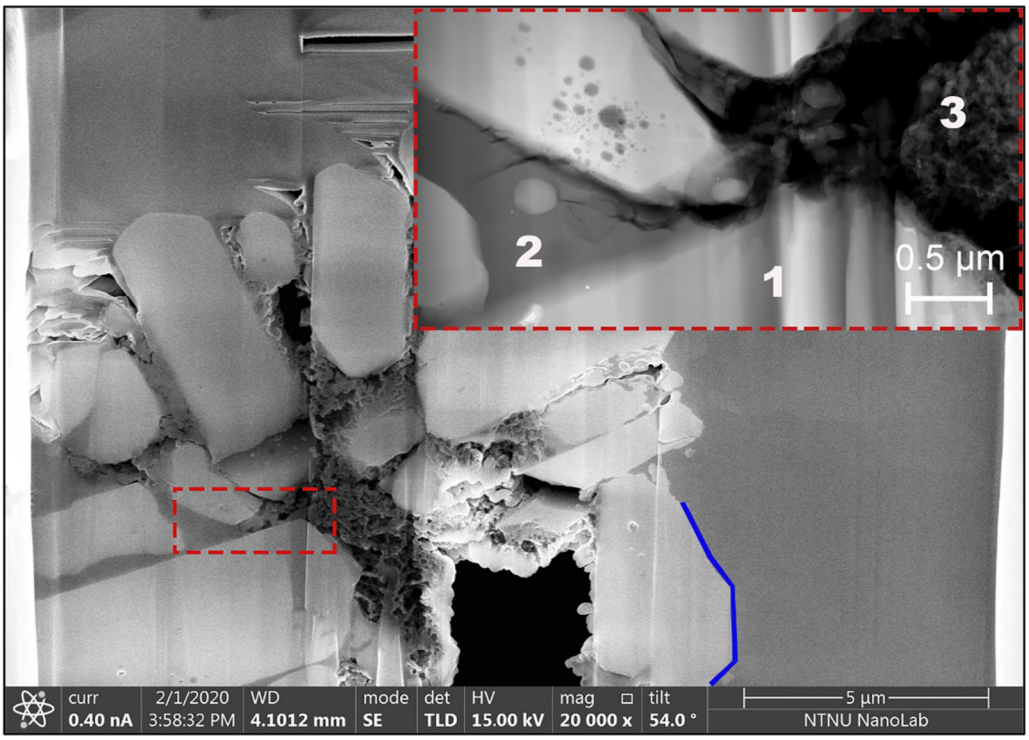

Fig. 20—A cross-section image of the filter–metal interface (marked with a blue solid line) between the Al_2O_3 + P1 filter and the pure aluminum. The sample was immersed in the pure aluminum for 120 min during the gravity priming procedure. The present image was retrieved from the bulk of the sample using a FIB, with subsequent element analysis of the following phases (from the section within the red dotted rectangles) using EDS: 1. alumina grains, 2. unmodified binder, and 3. reacted binder (Color figure online).

Table V. The Chemical Analysis of Phase 2 and 3 in Figure 20, Acquired by EDS from an Area of 0.3 × 0.3 μm^2 Using Transmission Electron Microscopy (TEM)

Element	Phase 2 [Weight Percent]	Phase 3 [Weight Percent]
Al	25	25
O	49	52
P	25	7
Mg	0	7

Al_2O_3 + P1 filter immersed in pure aluminum, as presented in Figure 17. Thus, the present result proves that reactions will occur between the filter and the aluminum melt even at very low concentrations of Mg.

IV. CONCLUSIONS

Three Al_2O_3-based ceramic foam filters were immersed in pure aluminum with traces of magnesium, as well as in an AlMg2 alloy, using two different experimental priming procedures with subsequent melt and filter analysis. Based on the trials performed, it was concluded that the phosphate-bonded filters (Al_2O_3 + P1 and Al_2O_3 + P2) suffered from binder degradation upon contact with an aluminum melt containing magnesium. The binder was observed to degrade at a magnesium concentration as low as 0.00035 wt pct, with the severity of the degradation increasing as the concentration of magnesium increased. Even the exposure time proved to have detrimental effect on the filter structure, with pieces of the filter struts breaking off and entering the melt. Clear changes in the melt composition in regard to phosphorus and magnesium were also observed, with an increasing concentration of phosphorus at the boundary layer between the filter and the metal, as well as in the molten metal itself, and an increased concentration of magnesium in the filter with a subsequent decrease in the melt. A clear color change in the filter from milky white to different gradients/shades of brown/black at the interface between the filter and the metal was the result of the chemical reaction between the aluminum melt and the phosphate-bonded filter material with subsequent release of phosphine gas exceeding the recommended exposure limits when in contact with the humidity in the air. Good agreement was established between the thermodynamic calculations performed using FactSage™ and the results of the experimental trials. As no degradation was observed in the case of the 100pctAl_2O_3 filter, there are strong indications that the degradation and phosphine gas formation was caused by the reactions between the phosphate-bonded filter material and the magnesium containing aluminum melt.

ACKNOWLEDGMENTS

The authors would like to thank the Research Council of Norway (NFR projectnr: 284090) and the German Research Foundation (DFG) for supporting

the present study as part of the Collaborative Research Centre 920 "Multi-Functional Filters for Metal Melt Filtration—A Contribution towards Zero Defect Materials." (Project-ID 169148856) subprojects A02. Furthermore, the authors would also like to acknowledge the support of Norsk Hydro ASA, the SELEE® Corporation, and the Department of Materials Science and Engineering at the Norwegian University of Science and Technology (NTNU).

FUNDING

Open access funding provided by NTNU Norwegian University of Science and Technology (incl St. Olavs Hospital - Trondheim University Hospital).

REFERENCES

1. K. Schwartzwalder and A.V. Somers: U.S. Patent No. 3 090 094A, United States Patent Office, 1963.
2. The Free Library: American Foundry Society Inc.: History of Ceramic Foam Filtration. (Aluminum Silver Anniversary Paper)., https://www.thefreelibrary.com/History+of+Ceramic+Foam+Filtration.+(Aluminum+Silver+Anniversary…-a0103795701, (accessed 18 September 2019).
3. M.J. Pryor and T.J. Gray: U.S. Patent No. 3 947 363A, United States Patent Office, 1976.
4. J.C. Yarwood, J.E. Dore, and R.K. Preuss: U.S. Patent No. 3 962 081A, United States Patent Office, 1976.
5. J.W. Brockmeyer: U.S. Patent No. 4 343 704, United States Patent Office, 1982.
6. D.C. Chesonis: *TMS Light Met*., 2017, pp. 1411–18.
7. H. Salmang and H. Scholze: 7th edn., Springer, 2007, p. 784.
8. A. Nishikawa: Plibrico Japan Company Limited, Tokyo, Japan, 1984, p. 109.
9. A.S. Wagh: 2nd edn., Elsevier, 2016, pp. 141–42.
10. A.P. Luz, M.A.L. Braulio, and V.C. Pandolfelli: 1st edn., Göller Verlag GmbH, 2015, pp. 214–16.
11. S. Schaafhausen, E. Yazhenskikh, A. Walch, S. Heidenreich, and M. Müller: *J. Eur. Ceram. Soc*., 2013, vol. 33, pp. 3301–12.
12. L.S. Aubrey, R. Olson, and D.D. Smith: *Mater. Sci. Forum*, 2009, vol. 630, pp. 137–46.
13. C.K.W. Solem, R. Fritzsch, and R.E. Aune: in *Extraction*, The Minerals, Metals & Materials Society, 2018, pp. 1153–63.
14. D.A. Doutre: *TMS Light Met*., 2010, pp. 797–800.
15. European Parliament and of the Council of the European Union: *Regulation (EC) No 1272/2008*, 2008.
16. National Institute for Occupational Safety and Health: Phosphine - Immediately Dangerous to Life or Health Concentrations (IDLH), https://www.cdc.gov/niosh/idlh/7803512.html, Accessed 17 September 2019.
17. Linde: Säkerhetsdatablad, https://www.linde-gas.se/sv/images/Fosfin_1.1_SE_tcm586-443518.pdf, Accessed 4 January 2021.
18. K. Sreenivasarao, F. Patsiogiannis, and J.N. Hryn: *TMS Light Met*., 1997, pp. 1153–58.
19. Y. Xiao, M.A. Reuter, and U. Boin: *J. Environ. Sci. Heal*., 2005, vol. 40, pp. 1861–75.
20. R. Fritzsch, M.W. Kennedy, J.A. Bakken, and R.E. Aune: *TMS Light Met*., 2013, pp. 973–79.
21. M.W. Kennedy, S. Akhtar, J.A. Bakken, and R.E. Aune: *Metall. Mater. Trans. B*, 2013, pp. 1–15.
22. M.W. Kennedy, S. Akhtar, R. Fritzsch, J.A. Bakken, and R.E. Aune: U.S. Patent No. 9 605 332B2, United States Patent Office, 2017.
23. Norwegian Meteorological Institute: Trondheim, statistics, https://www.yr.no/en/statistics/graph/1-211102/Norway/Trøndelag/Trondheim/Trondheim, Accessed 1 June 2020.
24. L.E. Nevander and B. Elmarsson: *Fukthandbok: Praktik Och Teori*, Svensk byggtjänst, Solna, 1994.
25. Drägerwerk AG & Co: Dräger-Tubes® for short-term measurements, https://www.draeger.com/en-us_us/Applications/Products/Portable-Gas-Detection/Gas-Detection-Tubes/Tubes/Short-term-Tubes, Accessed 12 December 2019.
26. C. Voigt, J. Hubálková, L. Ditscherlein, R. Ditscherlein, U. Peuker, H. Giesche, and C.G. Aneziris: *Ceram. Int*., 2018, vol. 44, pp. 22963–75.
27. E. Haugland, G.M. Haarberg, E. Thisted, and J. Thonstad: in *Essential Readings in Light Metals: Volume 2 Aluminum Reduction Technology*, G. Bearne, M. Dupuis, and G. Tarcy, eds., Springer International Publishing, Cham, 2016, pp. 229–33.
28. J.H. Kim, I.S. Kwon, K.M. Kim, C.H. Lee, and E.P. Yoon: *Mater. Sci. Technol*., 2000, vol. 16, pp. 243–48.